A Novel Ball Handling Mechanism for the RoboCup Middle Size League

Jeroen de Best*, René van de Molengraft and Maarten Steinbuch

Eindhoven University of Technology
Department of Mechanical Engineering
Control Systems Technology Group
P.O. Box 513, 5600 MB, Eindhoven, The Netherlands,
j.j.t.h.d.best@tue.nl, m.j.g.v.d.molengraft@tue.nl, m.steinbuch@tue.nl

Abstract

This paper presents the hardware design and control design of a novel ball handling mechanism in the RoboCup Middle Size League used by team Tech United Eindhoven. The ball handling mechanism consist of two levers with two actively driven wheels attached to it, to exert forces on the ball in order to control its position relative to the robot. The proposed design is fully compliant to the rules and regulations imposed by the RoboCup Middle Size League community. The control design consists of a cascaded velocity and position feedback loop in combination with a feedforward controller which compensates for the robots ego motion. The proposed design is validated on a robot used by the Tech United Eindhoven team.

Key words:
Motion control, Ball handling, RoboCup, Middle size league

*Corresponding author.

1. Introduction

This article presents a novel ball handling approach for the RoboCup [5] Middle Size League (MSL). In the MSL, where a team of autonomous robots play soccer, it is crucial to have a good ball handling during dribbling motion in order to maneuver fast through the defense of the opponents. Regarding ball manipulation the rules and regulations of the middle size RoboCup league [6] state that:

- The convex hull of the robot may enclose the ball only for one third of the ball diameter. During catching of the ball it may enclose half the diameter of the ball.
- The ball should rotate in its natural direction of rotation.
- Mechanical devices for ball manipulation, which in this work are referred to as ball handling mechanisms, are allowed provided that they are safe.

Obviously, the goal of ball handling mechanisms is to catch the ball and keep it during a dribbling motion of the robot, while satisfying the rules mentioned above.

Several methods for ball manipulation have been reported, e.g. [9, 3]. Many of the methods rely on passive systems in which the ball handling problem is shifted to a trajectory planning problem. In such systems only pushing forces can be exerted on the ball with a component pointing away from the robot. To slow down the ball the robot has to rotate 180 degrees around the vertical axis of the ball, which constraint is included in the trajectory planning. The other type of existing methods use active open-loop mechanisms

in which wheels or rollers spin backward in order to pull the ball towards the robot [3]. However, due to small variations in the friction between ball and field, the ball is prone to spinning backward or lying still during a forward movement. Touch sensitive ball handling is investigated in [15], where a combination of four sensors is implemented to give the robot the opportunity to have force and position feedback with respect to the ball. The closed loop control is still under investigation to improve the ball handling. Future work of [15] will focus on using the force and position measurements to adjust the path planning. However, no results have been presented yet. In [14] a ball handling design is described in which two wheels are used to actively exert forces onto the ball. The control architecture of [14] has two levels. On the low level the velocities of the wheels are controlled. At the high level a supervisory loop is implemented to determine whether or not the ball handling system needs to be activated such that the wheels are driven to match the velocity of the robot. However, there is no position measurement of the ball relative to the robot present to determine if the wheels are actuated correctly. When the ball has a slightly different radius for example the ball might spin backward and/or lies still during movements, which is against the prescribed rules and regulations.

The goal of this work is to present the mechatronic design approach of a novel active ball handling mechanism. The combination of the constructive hardware design and the motion control design have led to a multidisciplinary mechatronic concept which effectively solves the ball handling control problem. The novelty of the design lies in the fact that the presented active ball handling mechanism is closed-loop controlled in a sense that it controls the

distance between the ball and the robot. The proposed design is superior to the commonly used ones for multiple reasons. First of all, it creates the opportunity to drive *backwards* while still possessing the ball. Secondly, during a kick the ball can be pulled against the kicker or can be placed to the left or to the right of the kicker, which enables the robot to aim during a shot, without rotating the robot itself. Furthermore, during a dribbling movement the ball will rotate in its natural direction at all times, independent of the texture of the field or the ball. Finally, the trajectory planning problem becomes simpler since it not necessary to rotate around the vertical axis of the ball in order to change the direction during a dribbling motion.

In [2] a simplified theoretical approach regarding the proposed ball handling mechanism is given. Based on the same concept, we have extended this design in which a cascaded control structure, consisting of an inner velocity control loop and an outer position control loop, is applied instead of a single position control loop. As such, the operation flexibility is increased since even in cases where the ball is not in contact with the ball handling mechanism, the velocity of the wheels can still be controlled to save energy for example.

The rest of this paper is organized as follows. In Section 2 the robot of team Tech United Eindhoven will be explained on which the novel ball handling system is implemented. Sections 3 and 4 will discuss a simplified theoretical model of the ballhandling mechanism and the control design, while Sections 5 through 7 will discuss the practical implementation in detail. The control algorithm of the ball handling system used in practice, which will be explained in Section 5. Section 6 will present the autocalibration of the

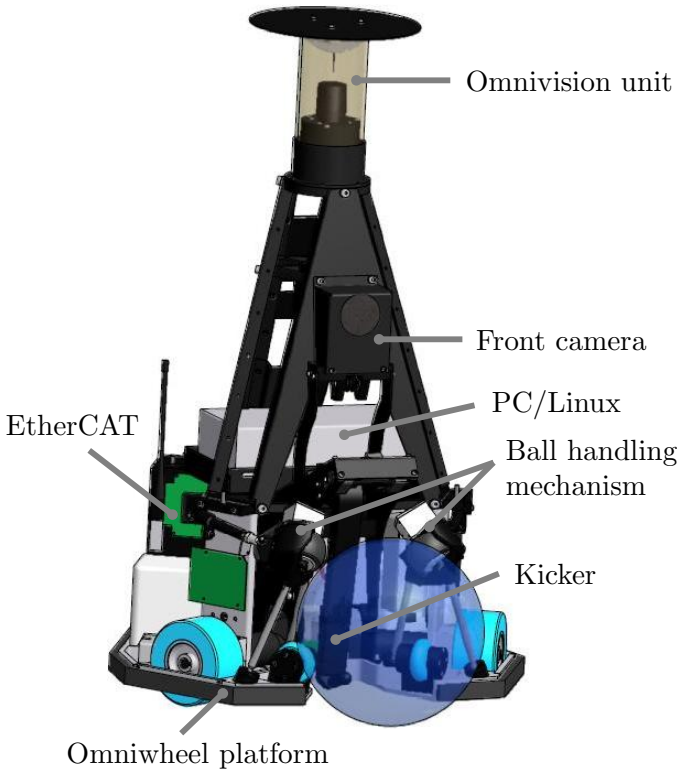

Figure 1: The soccer robot of team Tech United Eindhoven.

ball handling mechanism. The results of several tests will show the effectiveness of the proposed control design in Section 7. Finally, in the last section conclusions will be drawn and recommendations will be given.

2. Tech United Eindhoven robot

This section describes the Tech United Eindhoven robot, see Fig. 1, which acts as the testbed for the proposed control design. The robot movements are realized by three omniwheels. Each omniwheel is driven by a separate Maxon RE40 150 W DC motor fed by a Elmo Violin 25/60 current amplifier, which

can deliver 25 [A] continuous current. The position of the motor shaft is measured through a HEDL 5540 Maxon optical incremental encoder having 500 slits per turn. The motors are connected to the omniwheels via GP 42 C Maxon gear heads with a reduction of 49:4. For the purpose of ball kicking a solenoid is mounted [11], which delivers ball shots up to 10 m/s. The kicker is equipped with an adjustable mechanism in order to vary between a straight or lob shot or anything in between. The force exerted by the solenoid is controlled by PWM. The PWM signal together with the leg positioning enables the kicker to vary both ball velocity and angle. Like many other teams the robot is equipped with an omnidirectional camera that is used for ball and obstacle detection. The camera is a Gigabit Ethernet color camera of Prosilica, the GC750C, capable of capturing 752×480 images at a maximum rate of 60 Hz. A digital compass complements the omnivision system for the purpose of self localization. A VC4458 smart camera is mounted as a front camera, which will detect the ball when high lob shots are performed that cannot be detected by the omnivision system. Beckhoff [1] EtherCAT [4] modules are used for the real-time data acquisition. These modules are connected to an industrial PC running a 2.6.28.3 low-latency Linux kernel, which runs all control algorithms. The motion control is running at 1 kHz, whereas the image acquisition, image processing and team strategy algorithms run at 32 Hz.

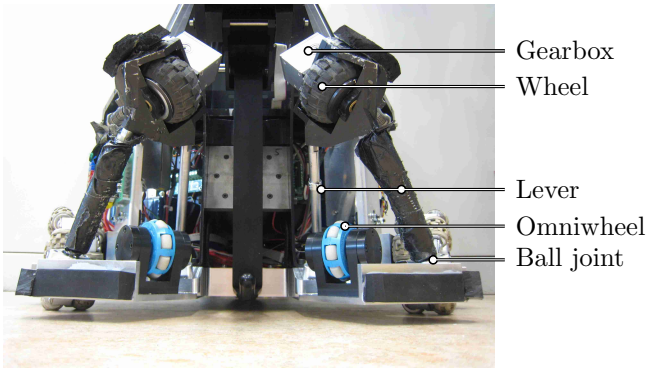

Figure 2: Front view of the ball handling mechanism.

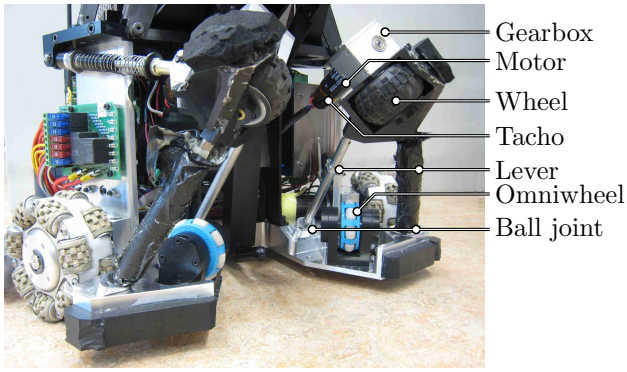

Figure 3: Side view of the ball handling mechanism.

Detailed figures of the ball handling mechanism are given in Fig. 2 and 3. The ball handling mechanism consists of two levers. Each lever consists out of two rods which are mounted on the base plate of the robot with rubber-cushioned ball joints such that the lever can rotate with respect to the base plate. During collisions the rubber is compressed such that an elastic deformation region is created to absorb the energy of the impact which increases the robustness of the mechanism against collisions. The angle of rotation

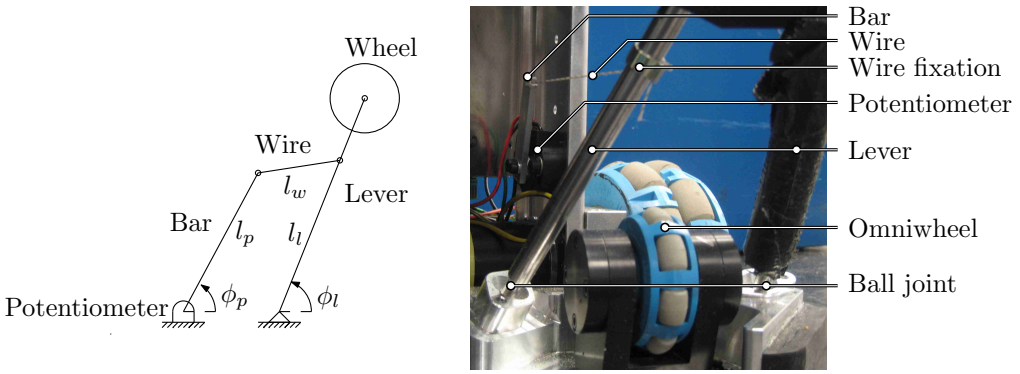

Figure 4: Schematic (left) and practical (right) angle measurement.

of the levers can be measured using potentiometers, see Fig. 4. A bar with length l_p is connected to a rotational potentiometer. This bar is connected to the lever using a wire with a length l_w. A spring in the potentiometer keeps the wire pretensioned. The length of the lever from the wire fixation to the ball joint is given by l_l. Using the lengths l_p, l_w and l_l a direct relation can be found between the measured angle of the potentiometer ϕ_p and the angle of the lever ϕ_l. A wheel driven by a motor is mounted on each lever. The wheels are driven by two Maxon RE25 20 W DC motors fed by Elmo Violin 5/60 current amplifiers, which can deliver 5 [A] continuous current. The velocity of the motor shafts can be measured through Maxon DCT 22 DC- tachometers. The motors are connected to the wheels via a Gysin GSR 12 perpendicular worm gearboxes with a reduction of 5:1. By applying a torque to the motors when the wheels are in contact with the ball, the levers will rotate forward or backward depending on the sign of the applied torque. Hence, the ball can be retracted or pushed forward with respect to the robot. This movement of the ball relative to the robot is measured by the poten-

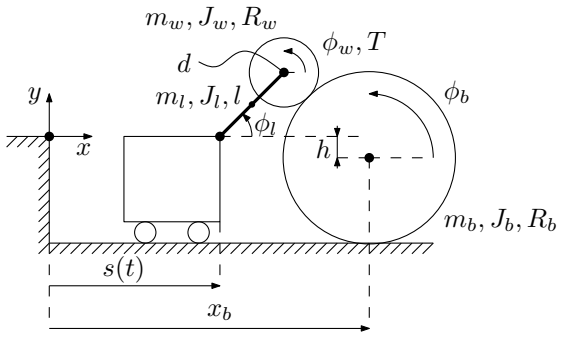

Figure 5: The active ball handling mechanism

tiometers. Therefore, we can created a closed-loop controlled system in which by applying a torque to the wheels the position of the ball with respect to the robot can be controlled.

One can imagine that during game play collisions with the other robots are, although not permitted, sometimes unavoidable. During these collisions high forces may be exerted on the ball handling levers, probably causing undesirable plastic deformations or even total fracture. The wheels are therefore partially covered with rubber foam to prevent cuts by sharp edges of other robots. The small omniwheels mounted on the base plate are used to create a fixed distance between the kicker and the ball, when the ball is fully retracted. This is important to be able to produce a reproducible shot.

3. Theoretical model

This section describes the theoretical model for the ball handling mechanism. The 2-dimensional simplified model of the ball handling mechanism is schematically depicted in Fig. 5. In this figure, the cart represents the soccer

robot. On the robot a lever is mounted that can freely rotate around a fixed point of the robot by means of a hinge. The height difference between this point and the center of the ball is denoted by h. The lever has a length l, a mass m_l and a rotational inertia J_l. At the end of the lever a wheel with mass m_w and rotational inertia J_w is mounted. The radius of the wheel is denoted by R_w. The wheel is driven by the motor torque T in the wheel bearing. This motor will be used to control the angle ϕ_l and to compensate for viscous damping (d) in the wheel. During dribbling the wheel is assumed to be in contact with the ball at all times. The ball has a radius R_b, a mass m_b and a rotational inertia J_b. Furthermore, it is assumed that there is no slip between wheel and ball nor between ball and floor. The motion of the robot is prescribed and is denoted by $s(t)$. The idea is to measure the angle of the lever ϕ_l and maintain this angle at a preferred angle, which corresponds to a desired distance between the ball and the robot. It will be shown that this can be realized by a feedback controller. The basic idea here is to apply a clockwise torque to retract the ball if the ball is too far away from the robot and to apply a counterclockwise to push the ball if it is too near.

In the remainder of this section the Lagrange's equations of motion for the system shown in Fig. 5 will be derived [7]. Therefore, the position vectors of the bodies' center of mass, i.e. $\underline{r}_l$, $\underline{r}_w$, $\underline{r}_b$ are derived as a function of the

generalized coordinate ϕ_l and the prescribed coordinate $s(t)$,

$$\underline{r}_l = \begin{pmatrix} s(t) + \frac{1}{2} l \cos(\phi_l) \\ \frac{1}{2} l \sin(\phi_l) \end{pmatrix}, \tag{1}$$

$$\underline{r}_w = \begin{pmatrix} s(t) + l \cos(\phi_l) \\ l \sin(\phi_l) \end{pmatrix}, \tag{2}$$

$$\underline{r}_b = \begin{pmatrix} s(t) + l \cos(\phi_l) + \sqrt{(R_b + R_w)^2 - (l \sin(\phi_l) + h)^2} \\ -h \end{pmatrix}. \tag{3}$$

Moreover, the rotation of each body, i.e. $\underline{\theta}_l$, $\underline{\theta}_w$, $\underline{\theta}_b$ can be calculated as a function of the generalized coordinate ϕ_l and the prescribed coordinate $s(t)$,

$$\underline{\theta}_l = \phi_l, \tag{4}$$

$$\underline{\theta}_w = \frac{s(t) + l \cos(\phi_l) + \sqrt{(R_b + R_w)^2 - (l \sin(\phi_l) + h)^2}}{R_w} - \frac{\arcsin\left(\frac{l \sin \phi_l + h}{R_b + R_w}\right)}{R_w}, \tag{5}$$

$$\underline{\theta}_b = \frac{s(t) + l \cos(\phi_l) + \sqrt{(R_b + R_w)^2 - (l \sin(\phi_l) + h)^2}}{R_b}. \tag{6}$$

The velocity vectors of the bodies can be calculated as

$$\underline{v}_l = \frac{d\underline{r}_l}{d\phi_l}\frac{d\phi_l}{dt} + \frac{d\underline{r}_l}{ds}\frac{ds}{dt} = \frac{d\underline{r}_l}{d\phi_l}\dot{\phi}_l + \frac{d\underline{r}_l}{ds}\dot{s}, \tag{7}$$

$$\underline{v}_w = \frac{d\underline{r}_w}{d\phi_l}\frac{d\phi_l}{dt} + \frac{d\underline{r}_w}{ds}\frac{ds}{dt} = \frac{d\underline{r}_w}{d\phi_l}\dot{\phi}_l + \frac{d\underline{r}_w}{ds}\dot{s}, \tag{8}$$

$$\underline{v}_b = \frac{d\underline{r}_b}{d\phi_l}\frac{d\phi_l}{dt} + \frac{d\underline{r}_b}{ds}\frac{ds}{dt} = \frac{d\underline{r}_b}{d\phi_l}\dot{\phi}_l + \frac{d\underline{r}_b}{ds}\dot{s}. \tag{9}$$

The rotational velocities can be calculated similarly

$$\underline{\omega}_l = \frac{d\underline{\theta}_l}{d\phi_l}\frac{d\phi_l}{dt} + \frac{d\underline{\theta}_l}{ds}\frac{ds}{dt} = \frac{d\underline{\theta}_l}{d\phi_l}\dot{\phi}_l + \frac{d\underline{\theta}_l}{ds}\dot{s}, \tag{10}$$

$$\underline{\omega}_w = \frac{d\underline{\theta}_w}{d\phi_l}\frac{d\phi_l}{dt} + \frac{d\underline{\theta}_w}{ds}\frac{ds}{dt} = \frac{d\underline{\theta}_w}{d\phi_l}\dot{\phi}_l + \frac{d\underline{\theta}_w}{ds}\dot{s}, \tag{11}$$

$$\underline{\omega}_b = \frac{d\underline{\theta}_b}{d\phi_l}\frac{d\phi_l}{dt} + \frac{d\underline{\theta}_b}{ds}\frac{ds}{dt} = \frac{d\underline{\theta}_b}{d\phi_l}\dot{\phi}_l + \frac{d\underline{\theta}_b}{ds}\dot{s}. \tag{12}$$

With these results the kinetic energy of the system becomes

$$K = \sum_{i\in\{l,w,b\}} \frac{1}{2} m_i \underline{v}_i^T \underline{v}_i + \frac{1}{2} J_i \underline{\omega}_i^T \underline{\omega}_i. \tag{13}$$

The potential energy can be written as

$$V = \frac{1}{2} m_l g l \sin(\phi_l) + m_w g l \sin(\phi_l) - m_b g h, \tag{14}$$

where g is the gravity constant.

With (13) and (14) the Lagrange's equations of motion can be calculated as

$$\frac{d}{dt}\left(\frac{dK}{d\dot{\phi}_l}\right) - \frac{dK}{d\phi_l} + \frac{dV}{d\phi_l} = Q_{nc}^T, \tag{15}$$

where Q_{nc} are the non-conservative forces. These forces consist of the applied torque T and the torque caused by the damping d between the lever and the wheel modeled as $T_d = d(\dot{\phi}_w - \dot{\phi}_l)$. These non-conservative forces are formulated as

$$Q_{nc} = \left(\frac{d\underline{\theta}_w}{d\phi_l} - \frac{d\underline{\theta}_l}{\phi_l}\right)(T_d - T). \tag{16}$$

Finally, a model, that is non-linear due the dependencies of ϕ_l in (1) through (3), can be constructed which has the form

$$\ddot{\phi}_l = f(\phi_l, \dot{\phi}_l, \dot{s}(t), \ddot{s}(t), T). \tag{17}$$

4. Control Design

Figure 5 shows a typical point of operation. Intuitively, one can see that such a point of operation is unstable. If there is no actuation, the lever will simply drop down due to gravity forces. In order to stabilize this operation point a feedback controller will be constructed based on a linearized model derived from (17). To further improve the tracking performance of the system, a feedforward controller will be designed as discussed in Section 4.2.

4.1. Feedback Design

In the previous section the non-linear model of the ball handling mechanism was derived. This section presents the design of a stabilizing feedback controller, i.e. a controller will be designed to control the angle ϕ_l by means of the torque T. Therefore, T will act as the input of the system, whereas ϕ_l will act as the output of the system. For the design of the feedback controller the non-linear model is linearized around the following desired equilibrium point

$$\phi_{l,eq} = \frac{\pi}{4},\ \dot{\phi}_{l,eq} = 0,\ \dot{s}_{eq} = 0,\ \ddot{s}_{eq} = 0,\ T_{eq}. \tag{18}$$

In the choice of this equilibrium point it is checked whether or not the chosen equilibrium point satisfies the preferred distance between the ball and the robot. Other equilibrium points may be chosen as well, since this does not influence the presented control method. The torque T_{eq}, associated with the chosen equilibrium point, can be calculated by substituting the values of (18) into (17) and solving for T_{eq} from

$$0 = f(\phi_{l,eq}\dot{\phi}_{l,eq}, \dot{s}_{eq}, \ddot{s}_{eq}, T_{eq}). \tag{19}$$

Linearization around the point of operating results in the following second order linear model

$$G : \begin{cases} \dot{\underline{x}} &= A\underline{x} + Bu \\ y &= C\underline{x} + Du \end{cases}, \tag{20}$$

where the state vector is given by $\underline{x} = \begin{bmatrix} \phi_l - \phi_{l,eq} & \dot{\phi}_l \end{bmatrix}^T$, the input u is given by $T - T_{eq}$ and the output y is defined as $\phi_l - \phi_{l,eq}$. The system matrix A, input matrix B, output matrix C and throughput matrix D are given by

$$A = \begin{bmatrix} 0 & 1 \\ \frac{df}{d\phi_l} & \frac{df}{d\dot{\phi}_l} \end{bmatrix}, B = \begin{bmatrix} 0 \\ \frac{df}{dT} \end{bmatrix}, C = \begin{bmatrix} 1 & 0 \end{bmatrix}, D = \begin{bmatrix} 0 \end{bmatrix}, \tag{21}$$

where A and B are both evaluated at the equilibrium point (18). The parameter values of the lumped model that correspond to the robot's behavior are given in Table 1:

With these parameters the linearized model G becomes

$$\begin{array}{rcl} \dot{\underline{x}} &=& \begin{bmatrix} 0 & 1 \\ 21.28 & -22.45 \end{bmatrix} \underline{x} + \begin{bmatrix} 0 \\ 757.24 \end{bmatrix} u \\ y &=& \begin{bmatrix} 1 & 0 \end{bmatrix} \underline{x} + \begin{bmatrix} 0 \end{bmatrix} u \end{array}. \tag{22}$$

The poles of this system are located at 0.91 and -23.36. The right half plane pole indicates that the considered system is indeed unstable.

Using the linearized model (20) single-input single-output control techniques can be applied in order to tune a feedback controller $\mathcal{K}$ that stabilizes the system around the equilibrium point, see Fig. 6. By using loop shaping techniques [12], a simple output feedback controller with a unity proportional gain can be used to stabilize the system given in (22). This feedback

Table 1: Parameters of the ball handling setup

Parameter	Description	Value	Unit
l	Length of the lever	0.07	[m]
m_l	Mass of the lever	0.3	[kg]
J_l	Inertia of the lever	$\frac{m_l l^2}{12}$	$\left[\text{kgm}^2\right]$
R_w	Radius of the wheel	0.028	[m]
m_w	Mass of the wheel	0.1	[kg]
J_w	Inertia of the wheel	$\frac{m_w R_w^2}{2}$	$\left[\text{kgm}^2\right]$
R_b	Radius of the ball	$\frac{0.69}{2\pi}$	[m]
m_b	Mass of the ball	0.43	[kg]
J_b	Inertia of the ball	$\frac{2m_b R_b^2}{3}$	$\left[\text{kgm}^2\right]$
d	Damping between lever and wheel	0.005	[Nmrad/s]
h	Height of rotation point of lever	0.035	[m]
g	Gravity constant	9.81	[m/s^2]

controller $\mathcal{K}$ is thus given by

$$u = e = r - y, \tag{23}$$

with the tracking error e defined as $e = r - y$. The set point of the controller is denoted by r. The closed loop poles are now given by -11$\pm$25i, hence a stable closed loop system is obtained.

With the designed feedback controller (23) a simulation is carried out in order to demonstrate the effectiveness of the proposed control design. The angle of the lever ϕ_l is initially set to $\frac{\pi}{8}$ [rad] while the soccer robot is in stand

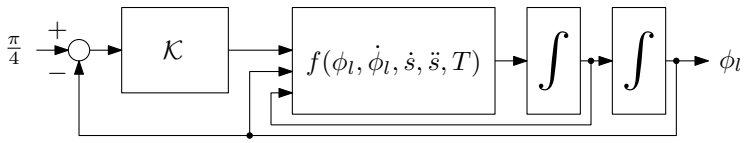

Figure 6: The control scheme.

still position, $s(t) = 0\ \forall t$. At $t = 0.5$ [s] the reference is set to $\frac{\pi}{4}$ [rad]. The results of this simulation are shown in Fig. 7. The figures on the left hand side show the responses of the angle ϕ_l as well as the angular velocity $\dot{\phi}_l$ for both the non-linear model, represented by a gray solid line, and the linear model, represented by a black dashed line. The figures on the right hand side reflect the differences between the non-linear model and linear model. From these figures it can be observed that the step reference results in a transient behavior at the output. The reference step is followed with an overshoot of 0.09 [rad] and a settling time of less than 0.2 [s]. Furthermore, it can seen that the difference between the non-linear model and linear model is very small. This justifies the use of a linear model for the control design.

4.2. Feedforward Design

In the previous section the operation point was chosen such that the acceleration of the robot is zero. In practice this will not be the case, since the robot will move constantly during a game. This brings us to the design of a feedforward controller, where we linearize the non-linear model around

$$\phi_{l,eq} = \frac{\pi}{4},\ \dot{\phi}_{l,eq} = 0,\ \dot{s}_{eq} = \dot{s}(t),\ \ddot{s}_{eq} = \ddot{s}(t),\ T_{eq}, \tag{24}$$

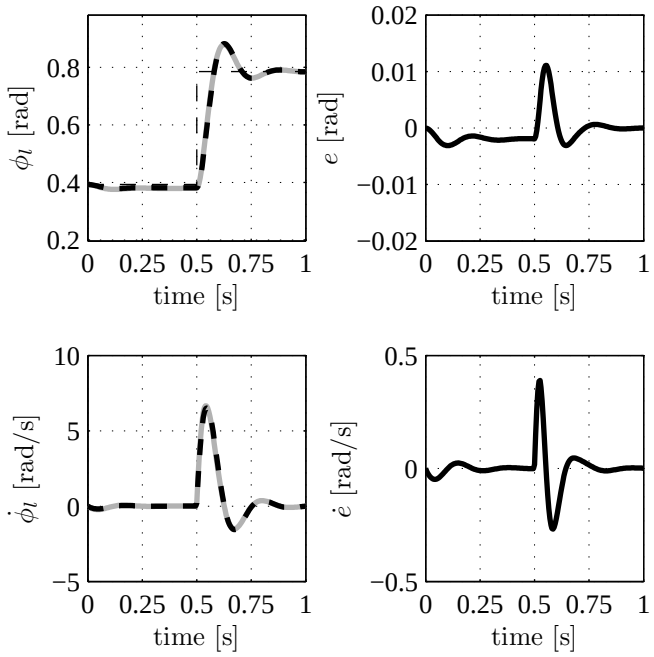

Figure 7: Step response of the closed-loop linear and non-linear model.

such that the torque T_{eq} will be a function of the velocity and acceleration of the robot, i.e. $T_{eq}(\dot{s}(t), \ddot{s}(t))$. Since the velocity $\dot{s}(t)$ and acceleration $\ddot{s}(t)$ are known we can calculate the torque T_{eq} and use it as a feedforward input in the control scheme to improve the tracking performance of the considered system. The total control scheme is schematically given in Fig. 8.

In the previous simulation the velocity of the robot was set to zero, $s(t) = 0 \; \forall t$. As can be imagined, this situation is rare during a soccer game.

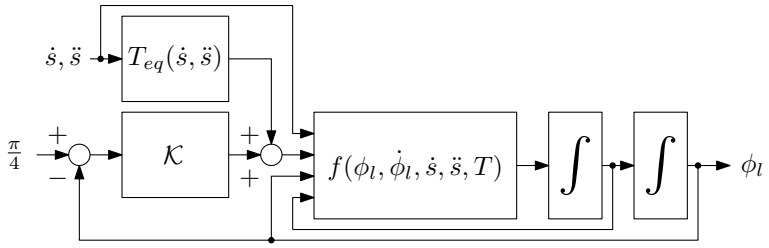

Figure 8: The control scheme with feedforward.

Therefore, another simulation is carried out while the robot is accelerating, $\ddot{s}(t) \neq 0$. From these simulations, the effectiveness of the feedforward controller is shown. In order to quantify the effect of the feedforward controller two simulations are carried out, one without feedforward controller and one with feedforward controller. During the simulation the robot is accelerating with 0.5 [m/s^2] and at $t = 0.5$ [s] again the reference is changed from $\pi/8$ [rad] to $\pi/4$ [rad]. The results of these simulations are shown in Fig. 9. The

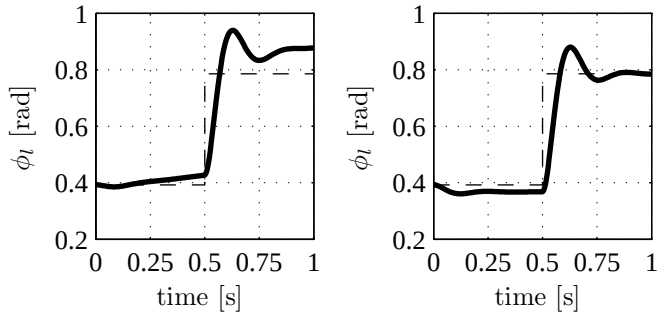

Figure 9: Step response of the closed-loop system during acceleration without feedforward (left) and with feedforward (right).

solid line in Fig. 9 is the response of the non-linear model (17). On the left

hand side the result without feedforward controller is shown, whereas on the right hand side the result of the simulation with feedforward controller is shown. It can be observed that if no feedforward controller is applied a non-zero error remains. This error is caused by the inertial forces of the bodies which act on the lever. Furthermore, the observed error is the result of the damping force that is generated when the wheel is turning with respect to the lever. The error is reduced by implementing the feedforward controller. This feedforward is of the form

$$T_{eq}(\dot{s}(t), \ddot{s}(t)) = a_2\ddot{s}(t) + a_1\dot{s}(t) + a_0, \tag{25}$$

where the coefficients $a_i, i \in \{0, 1, 2\}$ result from (24). From the results shown in Fig. 9 it can be seen that the tracking error of the reference angle vanishes due to the feedforward action.

The controller directly generates the torque of the ball handing wheel based on the lever angle error. This concept has been successfully validated in practice, see [2]. However, when the ball is not in the ball handling system, the error will be large, causing the wheels to spin hard. In these situations, it is preferable to control the velocities of the wheels, such that for example energy can be saved. Therefore, a major improvement with respect to the previous design will be discussed in which the velocities of the wheels can also be controlled when the ball *is not* in the ball handling mechanism. A cascaded control structure is adopted consisting of an inner velocity control loop and an outer position control loop, as opposed to the previous control design in which the wheel torques were directly calculated by the position feedback controller. The velocity of the wheels are controlled on the basis of the tachometers on the motors. This control design approach will be

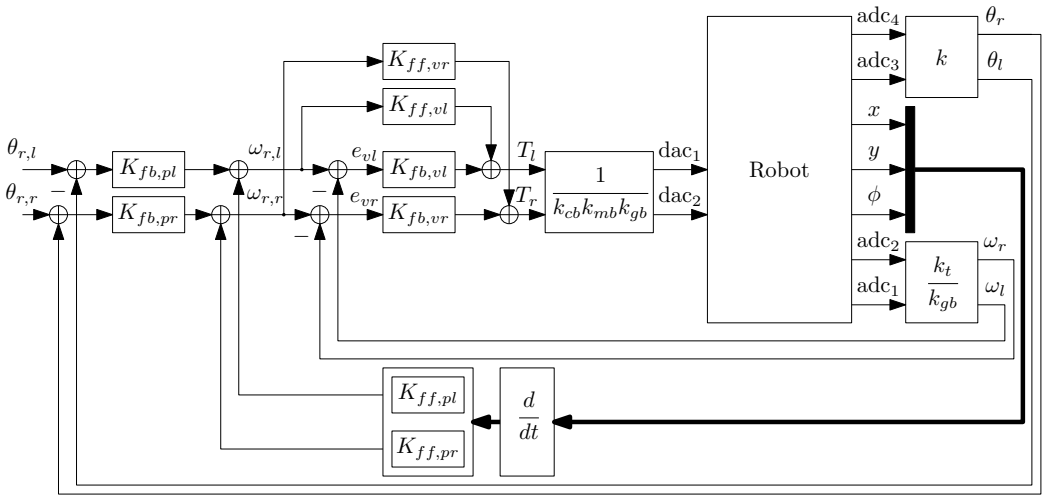

Figure 10: Hierarchical ball handling control scheme.

explained in the remainder of this paper.

5. Practical Control Design

The control architecture that is used in practice is a hierarchical one, see Fig. 10. On the low level, it consist of two velocity control loops to track the motor velocity references $\omega_{r,l}$ and $\omega_{r,r}$. The actual velocities are measured by the tachometers and are denoted by ω_r and ω_l. The analogue voltages of the tachos are measured through ADCs. The relations between the measured voltages and the angular velocities of the wheels are given by

$$\omega_l = \frac{k_t}{k_{gb}}\text{adc}_1, \tag{26}$$

$$\omega_r = \frac{k_t}{k_{gb}}\text{adc}_2, \tag{27}$$

where adc_1 and adc_2 are the measured voltages of the ADCs. The data sheet of the Maxon DCT 22 DC-tachometers states that it outputs 0.52 [V]

per 1000 [rpm]. Therefore, we define $k_t = \frac{2 \cdot \pi \cdot 1000}{0.52 \cdot 60}$ [rad/Vs] that relates the measured voltage to the velocity of the wheels in [rad/s]. The reduction of the Gysin GSR 12 perpendicular worm gearbox is $k_{gb} = 5$ [-]. The applied torques T_l and T_r are related to the DAC voltages according to

$$\text{dac}_1 = \frac{1}{k_{cb} k_{mb} k_{gd}} T_l, \tag{28}$$

$$\text{dac}_2 = \frac{1}{k_{cb} k_{mb} k_{gd}} T_r, \tag{29}$$

where dac_1 and dac_2 are the applied DAC voltages, $k_{cb} = \frac{5}{3.75}$ [A/V] is the gain of the current amplifier, $k_{mb} = 0.044$ [Nm/A] is the motor constant of the motors and $k_{gb} = 5$ [-] is the reduction factor. The two velocity control loops include two feedback controllers $K_{fb,vl}$ and $K_{fb,vr}$, and two feedforward controllers $K_{ff,vl}$ and $K_{ff,vr}$. The feedforward controllers consist out of mass feedforward, and friction feedforward.

On the high level, the control architecture contains two position control loops, one for each lever, to control the angles of the two levers. They contain the controllers $K_{fb,pl}$ and $K_{fb,pr}$. A preferred distance from the ball to the front of the robot can be defined, which results in preferred angles of the two levers $\theta_{r,l}$ and $\theta_{r,r}$. If the levers are bending forward a position error is introduced, which is controlled towards zero by adjusting the velocities of the wheels. If the levers are bending backward the wheels will spin in the opposite direction such that the ball is slightly pushed away from the robot. Since the robot also has to move, additional effort is necessary in order to maintain the levers at the preferred angle during these movements. This issue can be tackled by using feedforward. The input for the feedforward controllers $K_{ff,pl}$ and $K_{ff,pr}$ are the velocities (translational as well as rotational) of

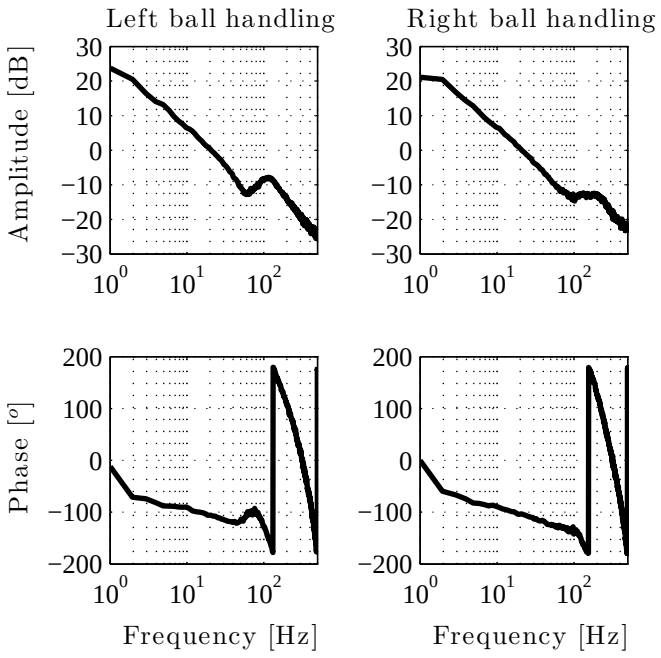

Figure 11: Measured frequency response function of the ball handling wheels.

the robot itself $\dot{x}$, $\dot{y}$ and $\dot{\phi}$, which can be derived from the on board motor encoders [16]. The design of the feedback and feedforward controllers will be explained in the next section.

5.1. Ball handling control design

The first step in the control design is to identify the plants for the velocity control loops. Therefore, two frequency response functions have been measured which are the transfer functions from the torques $T_l,\ T_r$ to the wheel velocities $\omega_l,\ \omega_r$. They are depicted in Fig. 11. It can be seen that the eigenfrequencies and damping of the two systems are not entirely the

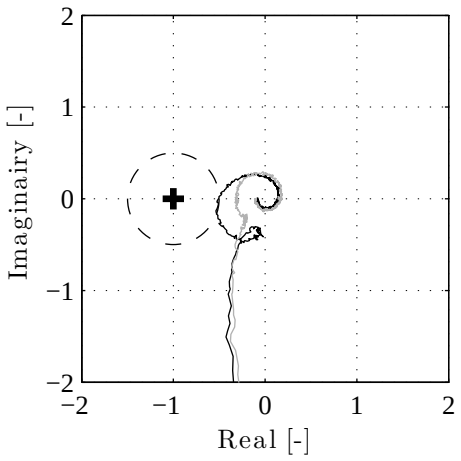

Figure 12: Open loop nyquist plots of the ball handling velocity control loops: left wheel (black), right wheel (gray).

same. Similar deviations can be expected if we measure these responses on different robots, i.e. we have to be robust with respect to these deviations. The feedback controllers that are designed are kept relatively simple and are proportional feedback controllers with a gain of 1.4,

$$K_{fb,vl} = K_{fb,vr} = 1.4, \tag{30}$$

resulting in bandwidths between 25 and 30 [Hz]. The nyquist plots of the open-loop systems are plotted in Fig. 12. As can be seen, in the worst case situation the modulus margin (inverse of the infinity norm of the sensitivity function), is around 0.5. This is indicated by the dashed circle around the point (-1,0) with a radius of 0.5.

The next step is to design the position feedback controllers $K_{fb,pl}$ and

$K_{fb,pr}$. Each motor influences the position of the ball with respect to the position of the robot. In order to apply SISO based controllers, we have to investigate the interaction of the 2×2 multi-input multi-output (MIMO) system. The amount of coupling between the two levers is minimized geometrically in this case by placing the levers under an angle of 90° with respect to each other. The plant as seen by the position controllers takes as input the reference velocities of the wheels $\omega_{r,l}$ and $\omega_{r,r}$ and has the measured angles of the levers θ_l and θ_r as outputs. The expectation is that the plant looks like a single integrator. The system contains a non-linear behavior similar to the classical example of an inverted pendulum. Although the system is non-linear, we assume small rotations, from which we can get a linearized model as described in [2]. To identify this model, a full MIMO frequency response function (FRF) is measured while the ball was in the ball handling mechanism. The amplitude of this FRF is given in Fig. 13. One can recognize the low level velocity control loop dynamics in this FRF. For low frequencies, up till approximately 10 [Hz], we see that the diagonal elements are pure integrators, whereas the off diagonal terms are small compared to the diagonal terms. Therefore, the expectation is, that the system is decoupled up to approximately 10 [Hz]. To check this, we use the relative gain array (RGA) [8]. The RGA provides a measure of interaction for MIMO systems, which is independent of input and output scaling. The RGA is defined as

$$RGA(G_d) = \Lambda(G_d) \equiv G_d \times (G_d^{-1})^T, \tag{31}$$

where $\times$ denotes element wise multiplication and G_d is the plant. In order to apply decentralized control it is preferred that this matrix is close to the unity matrix I for all frequencies. The RGA for our system is given in Fig. 14. The

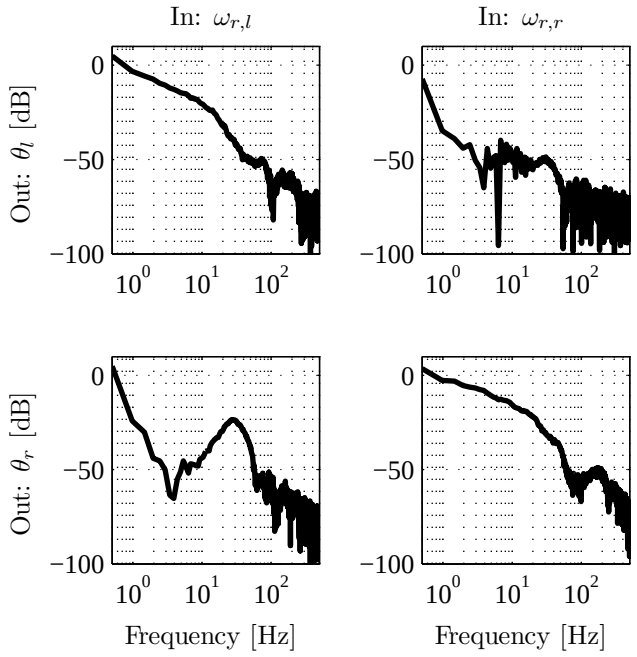

Figure 13: Measured frequency response function of the ball handling levers.

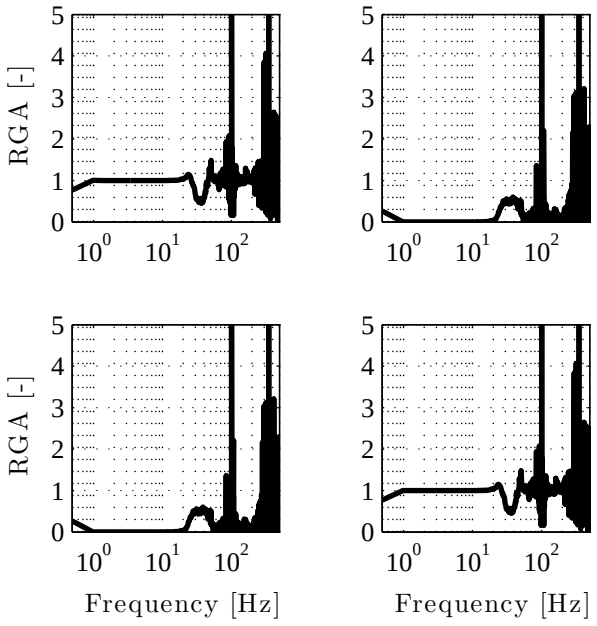

Figure 14: Measured relative gain array.

RGA also shows that the system is well decoupled until 20 [Hz]. Therefore, the bandwidth of the position control loop is taken to be smaller than this frequency. The implemented position controllers are proportional feedback controllers with a gain of one

$$K_{fb,pl} = K_{fb,pr} = 1. \tag{32}$$

With these controllers, the bandwidths of both position control loops are 1 [Hz].

The final step in the control design of the ball handling mechanism is

to design the feedforward controllers $K_{ff,pl}$ and $K_{ff,pr}$. These feedforward controllers compensate for the movement of the robot, i.e. the velocity of the robot is translated to angular velocities that the wheels nominally have to rotate. To determine this relationship a total number of 6 experiments have been carried out. During these experiments the robot is moved and a constant torque (no velocity control loops have been used here) is applied in order to keep the ball with the robot, but in such a way that the ball keeps rolling in a natural way. Hence, there is no feedback control of any kind present on the ball handling wheels during these experiments. The velocity of the robot is measured together with the velocities of both ball handling wheels. It is expected that the velocities of the wheels are related to the velocity of the robot by a direction dependent gain

$$\begin{pmatrix} \omega_l \\ \omega_r \end{pmatrix} = \begin{pmatrix} k_{11}(\text{sign}(\dot{x})) & k_{12}(\text{sign}(\dot{y})) & k_{13}(\text{sign}(\dot{\phi})) \\ k_{21}(\text{sign}(\dot{x})) & k_{22}(\text{sign}(\dot{y})) & k_{23}(\text{sign}(\dot{\phi})) \end{pmatrix} \begin{pmatrix} \dot{x} \\ \dot{y} \\ \dot{\phi} \end{pmatrix} = \begin{pmatrix} K_{ff,pl} \\ K_{ff,pr} \end{pmatrix} \begin{pmatrix} \dot{x} \\ \dot{y} \\ \dot{\phi} \end{pmatrix}. \tag{33}$$

By measuring the current velocity of the robot, we can feedforward angular velocities of the ball handling wheels. This is also depicted in Fig. 10. In the first two experiments the robot moves sideways, first in positive x direction, then in negative x direction. Next, positive and negative velocities were performed in y direction and ϕ direction. The results for the x direction are given in Fig. 15 through 18. In these figures, the measured angular velocities of the wheels are given in black, together with the velocity of the robot multiplied by the gain that is found given in gray. The gain k_{11} is

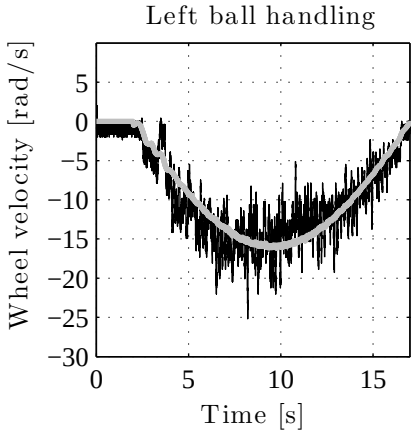

Figure 15: Open loop feedforward experiment for positive x direction, left ball handling measurement: ω_l (black), $k_{11}\dot{x}$ (gray)

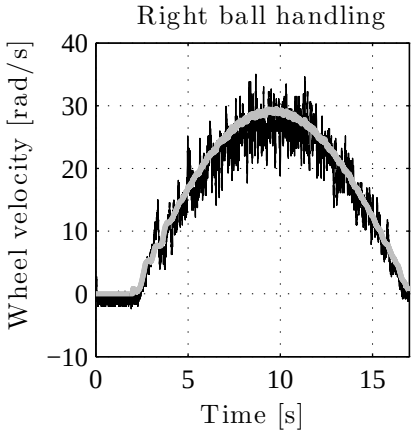

Figure 16: Open loop feedforward experiment for positive x direction, right ball handling measurement: ω_r (black), $k_{21}\dot{x}$ (gray)

determined to be

$$k_{11} = \begin{cases} -0.63 & \text{if } \dot{x} > 0 \\ -1.15 & \text{if } \dot{x} < 0 \end{cases}, \tag{34}$$

and the gain k_{21} is determined to be

$$k_{21} = \begin{cases} 1.15 & \text{if } \dot{x} > 0 \\ 0.63 & \text{if } \dot{x} < 0 \end{cases}. \tag{35}$$

Similar results are obtained for the y and ϕ directions. The gains k_{12} and k_{22} are found to satisfy

$$k_{12} = k_{22} = -0.82, \tag{36}$$

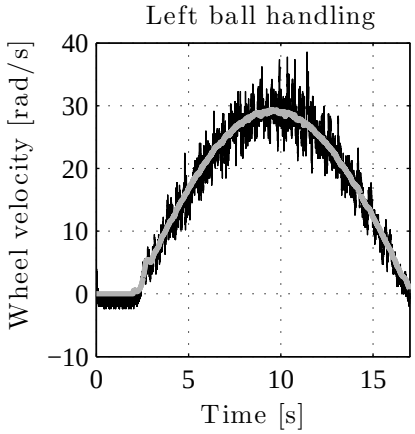

Figure 17: Open loop feedforward experiment for negative x direction, left ball handling measurement: ω_l (black), $k_{11}\dot{x}$ (gray)

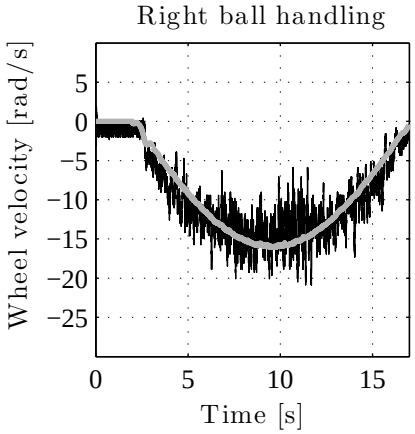

Figure 18: Open loop feedforward experiment for negative x direction, right ball handling measurement: ω_r (black), $k_{21}\dot{x}$ (gray)

whereas the gains k_{13} and k_{23} are given by

$$k_{13} = \begin{cases} 0.3 & \text{if } \dot{\phi} > 0 \\ 0.2 & \text{if } \dot{\phi} < 0 \end{cases}, \tag{37}$$

and

$$k_{23} = \begin{cases} -0.2 & \text{if } \dot{\phi} > 0 \\ -0.3 & \text{if } \dot{\phi} < 0 \end{cases}. \tag{38}$$

6. Auto calibration

As was already discussed, the angles of the ball handling levers are measured via potentiometers. During the assembly of the robot the sensors might be rotated due to mechanical imperfections. The measured stroke of

the levers is then the same, however the absolute values might differ. To be able to cope with this an auto calibration is implemented, which detects the begin and the end of strokes such that this stroke can be normalized. This is done as follows. When the robot is turned on, the lower position of the levers is measured for 1 second. The average of this signal is taken as the absolute reference angle 0. When the ball handling mechanism catches the ball, it pulls the ball with maximum force towards the robot for 100 ms. In this time span the strokes S_l and S_r are determined. In our case the strokes of the levers are 3.29 [V] and 3.09 [V], for the left and right lever, respectively. The stroke is limited by small (unactuated) omniwheels that are placed on the base plate of the robot, see Fig. 2 and 3. These omniwheels make sure that there is a fixed distance between the kicker and the ball. This is important to be able to produce a powerful but reproducible shot.

7. Results

The reference of the ball handling levers can now be set, which should satisfy $0 \leq \theta_{r,l} \leq S_l$ and $0 \leq \theta_{r,r} \leq S_r$. In our case the reference is set to $\theta_{r,l} = S_l - 0.3$ [V], and $\theta_{r,r} = S_r - 0.3$ [V]. It can be noted that the reference is chosen quite near the robot. The reason for this, is that in this situation we have a rather large controllable stroke before we loose the ball. If we choose the reference further away from the robot, the chance of losing the ball increases if disturbances, for example a collision with another robot, are present.

With these references, the first experiment that was done is to catch the ball. The results are given in Fig. 19 and Fig. 20. At $t = 1$ [s] the ball

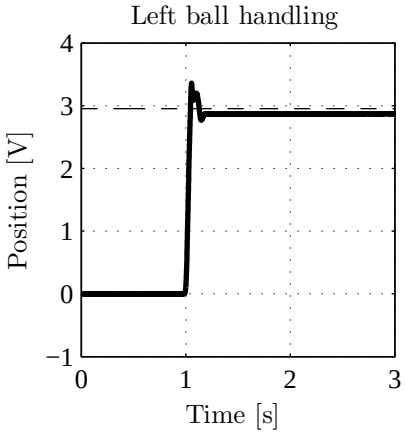

Figure 19: Catching of the ball: output (solid), reference (dashed).

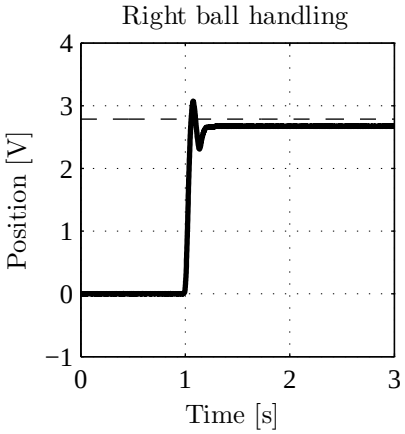

Figure 20: Catching of the ball: output (solid), reference (dashed).

approaches the robot and is catched by the ball handling mechanism. It can be seen from this figure that the ball handling mechanism reacts fast; the steady state position is reached within 0.25 [s]. However, it should be noted there is a steady state error of both lever angels, which is approximately 0.1 [V], (3% of the total stroke). An integrator in the controller could be implemented to reduce this steady state error, however one should be careful regarding integrator windup. This might occur when the ball is not in the ball handling mechanism for example. Therefore, it is chosen to keep the proportional controller.

Secondly, a test has been performed to evaluate the ball handling performance of the robot while the robot is moving. During the experiment the robot first has a positive velocity in y direction, then a negative velocity. Next, positive and negative velocities have been performed in x and ϕ direc-

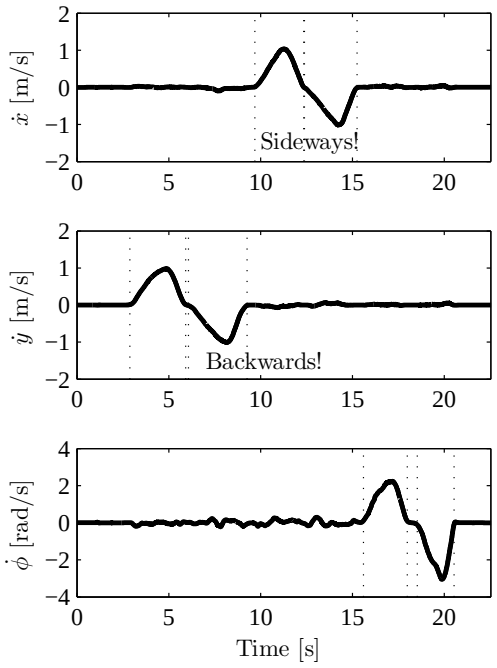

Figure 21: Movement of the robot.

tion. This can be seen in the Fig. 21, which shows the longitudinal, lateral and rotational velocities. The horizontal lines indicate the start and end of each movement. The measured outputs of the potentiometers are given in Fig. 22 and Fig. 23. From these figures we see that the wheels are actuated such that the ball is kept within the ball handling mechanism. If this was not the case the output would drop to 0 [V], i.e. the levers would be in forward position. It can be observed that during x and ϕ movements the errors are larger than for the y direction. This is caused by the fact that the resulting force that the wheels exert on the ball is right through the center of the ball in case of the y direction, whereas in case of the x and ϕ direction it is not,

so also a torque on the ball is introduced in that case. To see the effect of the feedforward control a similar experiment is carried out without the use of feedforward based on the velocity of the robot, i.e. $K_{ff,pl} = K_{ff,pr} = 0$. The results are given in Fig. 24 and Fig. 25. From these figures we see that without the use of feedforward the ball is lost, three times in this case. This is the case when the values drop to 0 [V]. What can not be observed from these figures, is that the ball was not rolling during a forward movement (positive y direction), which is not allowed. Also, the end of stroke is reached many times. This can be recognized by flat curves above the references in Fig. 24 and Fig. 25. These are not present in the case the feedforward is present.

8. Conclusions

In this paper a novel ball handling approach was presented as used by MSL team Tech United Eindhoven. A theoretical model was given, together

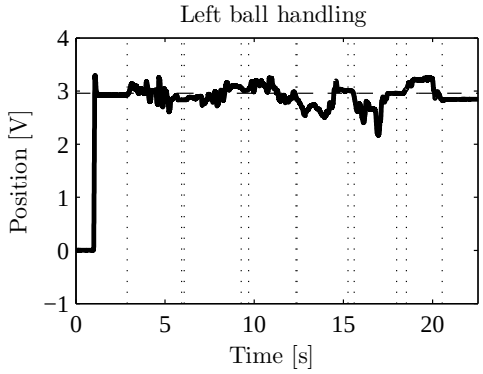

Figure 22: Control of the ball: output (solid), reference (dashed).

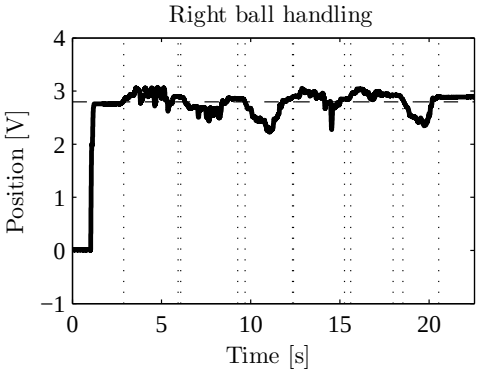

Figure 23: Control of the ball: output (solid), reference (dashed).

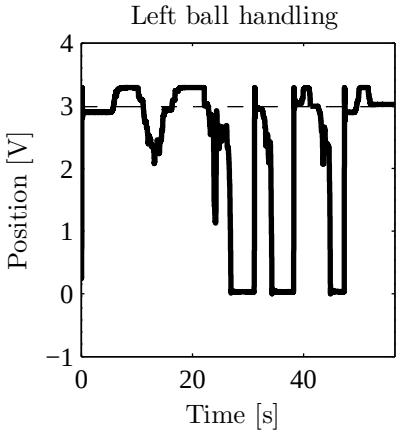

Figure 24: Control of the ball without feedforward: output (solid), reference (dashed).

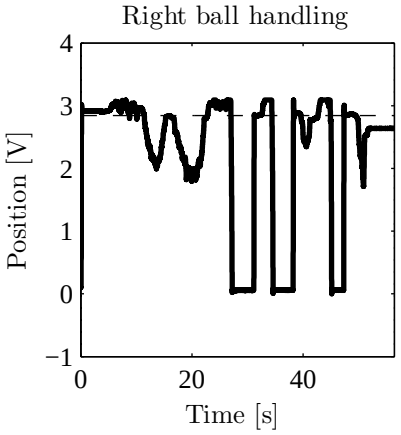

Figure 25: Control of the ball without feedforward: output (solid), reference (dashed).

with a stabilizing controller. In practice, a cascaded control strategy is implemented, which on the low level controls the velocity of the wheels of the ball handling mechanism, whereas on the high level a position control loop is used. The effectiveness of the proposed control algorithm is shown in practice: the distance from the ball to the robot can be controlled within the range of the ball handling mechanism even during side movements and rotations. During all movements the ball keeps rolling in the natural rolling direction as stated by the rules. Using the longitudinal, lateral and rotational velocity information of the robot, a feedforward controller is constructed that determines the nominal velocity that the wheels should rotate as a function of the robot's velocity. The experimental results show that the implementation of the feedforward controllers leads to a performance increase. The ball

is not lost anymore and ball pushing, where the ball does not rotate while the robot is moving, does not happen anymore.

To further improve the tracking performance a feedforward controller was implemented leading to a significant decrease of the tracking error of the preferred reference angle. Future research will focus on the possibilities for aiming the ball before shooting without rotating the robot itself which can be achieved by altering the reference angles of the levers. Another possibility is soft kicking or passing with the ball handling mechanism instead of the kicker which is to be investigated in near future.

References

[1] Beckhoff, *EtherCAT, Ultra high-speed communication*, http://www.beckhoff.de/english.asp?ethercat/default.htm, 2009.

[2] J. de Best and R. van de Molengraft, An Active Ball Handling Mechanism for RoboCup, International Conference on Control, Automation, Robotics and Vision, pp. 2060-2065, Hanoi, 2008.

[3] R. D'Andrea, T. Kalmar-Nagy and P. Ganguly, M. Babish, *The Cornell RoboCup Team* in RoboCup 2000: Robot Soccer World Cup IV, P.Stone, T. Balch and G. Kraetzschmar, Eds., New York: Springer, pp. 41-51, 2002.

[4] D. Janssen, H. Buttner, *Real-time Ethernet the EtherCAT solution*, Computing and Control Engineering Journal, vol 15, no 1, 2004.

[5] RoboCup, RoboCup Official site, www.robocup.org, 2009.

[6] MSL Technical Committee 1997-2008, *Middle Size Robot League Rules and Regulations for 2008*, draft version 12.2 20071109, 2007.

[7] A. de Kraker and D.H. van Campen, *Mechanical Vibrations*, Shaker Publishing BV, ISBN 90-423-0165-1, 2001.

[8] S. Skogestadt and I. Postlethwaite, *Multivariable Feedback Control, Analysis and Design (2nd Edition)*, Wiley, ISBN 13-978-0-470-01168-3, 2007.

[9] S. Stancliff, *Evolution of Active Dribbling Mechanisms in RoboCup*, 16-741 Project, April, 2005.

[10] Tech United Eindhoven, Technische Universiteit Eindhoven: Tech United Eindhoven, http://www.techunited.nl, 2009.

[11] R. Tilburgs, *Design and realization of a solenoid for a RoboCup kicking device*, DCT 2006.120, Internal Report, Technische Universiteit Eindhoven, 2006.

[12] G.F. Franklinn, J.D Powell and A Enami-Naeihi, *Feedback Control of Dynamic Systems*, Addison-Wesley Publishing Company, ISBN 0-201-52747-2, 1994.

[13] Data sheet of Gysin worm gearboxes, `http://www.gysin.com/fileadmin/user_upload/Dokumente/GSR12_e.pdf`.

[14] NuBot Team Description Paper 2009, RoboCup 2009 Graz, CD-ROM, Graz, Austria, July, 2009.

[15] Mostly Harmless Team Description Paper 2009, RoboCup 2009 Graz, CD-ROM, Graz, Austria, July, 2009.

[16] K. Watanabe, Y. Shiraishi, S.G. Tzafestas, J. Tang and T. Fukuda, *Feedback Control of an Omnidirectional Autonomous Platform for Mobile Service Robots*, Journal of Intelligent and Robotic Systems, vol. 22, pp. 315-330, 1998.